Original Article

MOLECULAR METABOLISM

cAMP-MicroRNA-203-IFNγ network regulates subcutaneous white fat browning and glucose tolerance

Xiaolong Guo [1], Zhichun Zhang [1,2], Ting Zeng [1], Yen Ching Lim [2], Yumeng Wang [1], Xinxin Xie [1], Song Yang [1], Chenglong Huang [1], Min Xu [1], Linfen Tao [1], Hongxiang Zeng [1], Lei Sun [2,], Xi Li [1,*]**

ABSTRACT

Objective: Brown and beige adipocytes in humans and rodents are specialized to burn lipids for heat generation as a natural defense against cold and obesity, which is advantageous to metabolic homeostasis. MicroRNAs as another regulatory layer to regulate metabolic homeostasis attracted a lot of attentions. Our previous work revealed microRNA (miR)-203 as a brown adipocyte-enriched microRNA involved in brown adipocytes development. However, the potential role of miR-203 in adipose tissue metabolic homeostasis has not been determined *in vivo*. In this study, we investigate the potential role of miR-203 in subcutaneous white adipose tissue (sub-WAT) browning and metabolic homeostasis.

Methods: We investigated the relationship between miR-203 and energy homeostasis in adipose tissue from cold exposed, high fat diet (HFD) fed, ob/ob and db/db mice. The functions of miR-203 on sub-WAT browning were validated through miR-203 knockdown or overexpression. The miR-203 targeted signal pathway was screened by RNAseq analysis. Luciferase report assay, western blot, and qPCR were performed to establish the miR-203 related upstream and downstream signal pathway *in vivo* and in *vitro*. The functions of miR-203 on obesity and metabolic homeostasis were validated through GTT/ITT and western blot on high fat diet-induced obesity in C57 mice. ELISA was used to determine the concentration of IFN-γ. Flow cytometry analysis was performed to determine the infiltration of macrophages in adipose tissue.

Results: MiR-203 expression positively correlates with energy expenditure, and overexpression of miR-203 could enhance sub-WAT browning in normal diet (ND) condition. Mechanistically, the expression of miR-203 is activated by cAMP-dependent C/EBPβ up-regulation. Subsequently, miR-203 inhibits IFN-γ signal pathway activation by directly targeting Lyn, which is an activator of Jak1-Stat1. Moreover, the forced expression of miR-203 could improve insulin sensitivity and resist high fat diet-induced obesity by inhibiting IFN-γ.

Conclusions: MicroRNA-203 (miR-203) promotes white adipose tissue browning in cold exposed mice and improves glucose tolerance in HFD fed mice by repressing IFN-γ. Since miR-203 is activated by cAMP-dependent C/EBPβ up-regulation and directly represses IFN-γ signal pathway, we declare that miR-203 acts as a messenger between cAMP signal pathway and IFN-γ signal pathway.

© 2019 The Authors. Published by Elsevier GmbH. This is an open access article under the CC BY-NC-ND license (http://creativecommons.org/licenses/by-nc-nd/4.0/).

Keywords MiR-203; cAMP signaling; IFN-signaling; Thermogenesis; Glucose tolerance

1. INTRODUCTION

The prevalence of obesity with a high risk of metabolic dysfunction is a health burden all over the world [1,2]. However, available treatments for obesity are limited. Rodents and humans possess at least two populations of Ucp1-positive thermogenic adipocytes: classical brown adipocytes and beige adipocytes [3,4]. Beige adipocytes reside within white adipose tissue and usually emerge in response to chronic cold exposure and physical exercise [5]. This kind of Ucp1 positive adipocyte exhibits BAT-like qualities, multilocular lipid droplet morphology, higher mitochondrial content, and thermogenic capacities which increase energy expenditure and defend against obesity [6,7].

A variety of transcriptional regulators such as C/EBPβ, PPARγ, and PRDM16 control the brown- and beige-selective thermogenic gene program [8]. Additionally, a new class of regulatory molecules, miRNAs, are reported to regulate metabolic homeostasis through interacting with transcriptional control mechanisms [8–10]. In particular, several miRNAs have recently emerged as important regulators of brown and beige adipocyte differentiation and function [11,12]. Meanwhile, our previous work revealed that microRNAs were required for the feature maintenance and differentiation of brown adipocytes [13]. With microarray analysis, we identified miR-203 as a brown fat-enriched microRNA. Inhibition of miR-203 in primary brown adipocytes resulted in impaired brown adipogenesis [13]. However, the function of miR-203 on fat metabolism has not been determined *in vivo* and the mechanism by which miR-203 regulates adipose tissue thermogenesis is not known.

[1]Biology Science Institutes, Chongqing Medical University, PR China [2]Cardiovascular and Metabolic Disorders Program, Duke-NUS Medical School, Singapore

*Corresponding author. Chongqing Medical University, 1 Yi Xue Yuan Road, Chongqing, 400016, PR China. E-mail: lixi@shmu.edu.cn (X. Li).

**Corresponding author. Cardiovascular and Metabolic Disorders Program, Duke-NUS Medical School, 169857, Singapore. E-mail: sun.lei@duke-nus.edu.sg (L. Sun).

Received May 7, 2019 • Revision received June 17, 2019 • Accepted July 2, 2019 • Available online 6 July 2019

https://doi.org/10.1016/j.molmet.2019.07.002

 © 2019 The Authors. Published by Elsevier GmbH. This is an open access article under the CC BY-NC-ND license (http://creativecommons.org/licenses/by-nc-nd/4.0/).

Lately, an important study reveals that targeting neuro-innate signaling between the sympathetic nervous system and the immune system may offer new approaches to mitigate chronic inflammation-induced metabolic impairment [14]. We know that sympathetic neurons exocytose catecholamines, leading to cyclic AMP (cAMP) enrichment and fat burning, characterized by the up-regulation of Ucp1 [15,16]. Additionally, it is reported that IFN-γ signaling severely disturbs the white-to-brown conversion [17,18] and metabolic homeostasis by increasing the adipose inflammation response [19,20]. However, the relationship between the sympathetic nervous system and the IFN-γ signaling pathway remains unclear.

Here we show that knockdown of miR-203*in vivo* significantly impairs subcutaneous white fat browning, while overexpression of miR-203 promotes the browning process under ND condition. The expression of miR-203 is transcriptionally wired into the thermogenic program by C/EBPβ during cAMP signaling activation. Subsequently, miR-203 repressesthe IFN-γ signal pathway via the tyrosine-protein kinase Lyn, an activator of Jak1-Stat1 [21]. Importantly, overexpression of miR-203 can improve insulin sensitivity and prevent high fat diet-induced obesity. Hence, we report that miR-203 could promote subcutaneous white fat browning and that miR-203 has a beneficial effect on metabolic homeostasis.

2. MATERIALS AND METHODS

2.1. Animals and treatment

Four to six-week-old male C57BL/6J mice were purchased from the Experimental Animal Center of Chongqing Medical University (Chongqing, China). Mice were maintained under 12-hour light/12-hour dark cycles and fed with ND or HFD (60% kcal in fat, beginning at age 6 week). CL-316243 disodium salt (sigma) was administered via daily intraperitoneal injection (1 mg kg^{-1}) for a week. 8-weekold mice were treated with Locked Nucleic Acids (LNAs) microRNA inhibitors (8 mg kg^{-1}) (Exiqon), adenovirus (1×10^8 to 10^{10} PFU), or Saracatinib (25 mg kg^{-1}) (Selleck) into inguinal fat pat. Adenovirus constructs were designed from our laboratory; for more details, please refer to the adenovirus section. All studies were approved by the Animal Care and Use Committee of the Chongqing Medical University and followed the National Institute of Health guidelines on the care and use of animals.

2.2. Adipose stromal vascular fraction cells isolation and culture

The stromal vascular fractions (SVFs) cells from white fat tissue and brown fat tissue were isolated as described before with few modifications [22]. Briefly, minced tissue depots were treated with 0.2% collagenase (Sigma) digestion at 37 °C for 25–30 min. Digested tissues were filtered through a 100 μm mesh filter. After centrifugation, the mature adipocytes floating above on the supernatant, and cellular pellet involving the SVFs was resuspended with an ammonium chloride lysis buffer to remove red blood cells. Both SVFs and adipocytes were washed with 0.5% calf serum in phosphate-buffered saline (PBS). The freshly isolated SVFs cells were seeded and cultured in DMEM containing 10% FBS (Gibco)and 0.5% penicillin/streptomycinat 37 °C with 5% CO_2. On confluence, the cells were induced to differentiate for 2 days with DMEM containing 10% FBS, 5 μg/mlinsulin (Roche),1 μmol/Ldexamethasone (Sigma), 0.5 mmol/L of 3-isobutylmethylxanthine (Sigma) and 5 μmol/L rosiglitazone (Sigma). The induction medium was replaced with DMEM containing 10% FBS and5 μg/ml insulinfor 2 days. Then cells were incubated in DMEM with 10% FBS.

2.3. Cell culture

For 3T3-L1 induction and treatment, 3T3-L1 preadipocytes were propagated and maintained in DMEM containing 10% calf serum (CS; Gibco). Two days post-confluence (designated day 0), cells were induced to differentiate with DMEM containing 10% FBS (Gibco), 1 μg/ml insulin, 1 μmol/L dexamethasone, and 0.5 mmol/L 3-isobutyl-1-methylxanthine until day 2. Cells were fed DMEM supplemented with 10% FBS and 1 μg/ml insulin for 2 days and then incubated in DMEM with 10% FBS. Expression of adipocyte genes and acquisition of adipocyte phenotype began at day 3 and reached a maximum at day 6. For drug treatment, cells were incubated with 50 μmol/L forskolin (Sigma) or 10 μmol/L isoproterenol (Sigma) for 6–8 h for RNA and protein analyses, respectively.

For T cell culture with conditional medium, Jurkat immortalized human T cellswere cultured in RPMI 1640 medium (Gibco) containing 10% FBS (Gibco) and maintained in 5% CO2 at 37 °C. For the adipocytesconditional medium, 3T3-L1 preadipocytes were induced to differentiation as described above. Ad-miR-203 and Ad-Vector were transfected at the fourth day after induction, respectively. Cells were then washed and fresh medium was replaced after 24 h. The medium was then collected at the seventh day after induction. The conditional medium was filtered and used at a 1:1dilution with fresh medium for T cell culture; cells were collected for RNA and protein analyses after 48 h.

2.4. Adenovirus constructs

The miR-203 knockdown adenovirus was constructed by using a BLOCK-iT™-U6-Entry-Vector (Invitrogen) according to manufacturer's instructions. The miR-203 overexpression adenovirus was constructed by using an pDC316-mCMV-EGFP-vector (Biowit, Shenzhen, China) according to manufacturer's instructions. The overexpression adenovirus vector was a generous gift from the Dr. Li Gang lab.

Overexpression vector insert sequence: CAGGAGGGCGCTGAGCTGTGGCTCCGGAGCTCCGGGCTGTGCAGAACTTCTGTGTGCAGGCGCGCCTGGTCCAGTGGTTCTTGACAGTTCAACAGTTCTGTAGCACAATTGTGAAATGTTTAGGACCACTAGACCCGGCGCGCACGGCGGCGACGACAGCAGCGACGGGGCGGCCCCGACGGCCAAGGTCGGCTTGAGAGGGGCGCGGGGGTGGGGTGGGGGCACCCGGATCGCCGAGACTCG.

Knockdown vector insert sequence: CACCGCTAGTGGTCCCCACATTTCACCGATCTAGTGGTCCCCACATTTCACACCGGTCTAGTGGTCCCCACATTTCACTCACCTAGTGGTCCCCACATTTCAC.

2.5. Adenovirus amplification and purification

The adenovirus was amplified in 293A cells. In brief, 293A cells cultured in 10% fetal bovine serum about 90% confluence were added with adenovirus seed. 48 h post-infection, visible regions of cytopathic effect (CPE) are observed. Harvest adenovirus stock until approximately 70% CPE is observed (typically 3 days post-infection). Frozen at −80 °C for long-term preservation, the adenovirus stock was purified by Adenovirus Purification Kits (Sartorius, UK) according to manufacturer's instructions.

2.6. Western blotting and antibodies

Tissue homogenate or cellslysate in lysis buffer containing 2% SDS and 50 mM Tris–HCl (pH6.8). Lysates were then quantitated and equal amounts of protein were subjected to SDS-PAGE and immunoblotted with antibodies against β-actin, Ucp1, C/EBP-β, Jak1, Stat1, and Lyn. Antibodies against β-actin (4967s) and Lyn (2796s) were from Cell SignalingTechnology, antibodies against Stat1 (sc-346) were from Santa Cruz Biotechnology, antibodies against Jak1 (ab133666) and

 © 2019 The Authors. Published by Elsevier GmbH. This is an open access article under the CC BY-NC-ND license (http://creativecommons.org/licenses/by-nc-nd/4.0/).

Ucp1 (ab23841) were from Abcam, and antibodies against C/EBP-β were from the Department of Biological Chemistry, Johns HopkinsUniversity School of Medicine.

2.7. RNA-seq analysis

Sequencing reads were first aligned against mm10 using tophat-2.0.11 [23] followed by gene quantification into FPKM units using cufflinks-2.1.1 [23]. Lowly expressed protein-coding genes (Average FPKM $\leq$ 1) in both control and miR-203 inhibition groups were filtered off from all downstream analyses. For the remaining set of genes, we adjusted the basal average expression to FPKM 1 and used for all downstream analyses thereafter. Statistical analysis for differential gene expression was performed using Cuffdiff [24]. Genes were considered significantly differentiated when q-value $<$0.05 and fold change of at least 1.5.

2.8. Gene set enrichment analysis

GSEA [25] was performed on a pre-ranked $\log_2$ (mir-inhibition/control) list and compared against "GO gene sets" (C5) from MsigDB [25,26]. Redundant enriched gene ontologies were removed using REVIGO [27] with default parameters.

2.9. Quantitative real-time PCR assay

Total RNAs were extracted with TRIzol (Invitrogen). For mRNA analysis, 1 μg total RNAs was reverse transcribed by using a Revert Aid first strand cDNA synthesis kit (Thermo Scientific). The cDNA was analyzed using the Power SYBR green PCR master mix (Applied Biosystems, Carlsbad, CA) with the ABI Prism 7500 qPCR machine (Applied Biosystems). mRNA qPCR data were normalized to the rpl23.

For miRNA analysis, 8 ng total RNAs was reverse-transcribed, and qPCR was operated with particular TaqMan primers according to the manufacturer's instruction (Applied Biosystems). miRNA qPCR data were normalized to the snoRNA202. Details of primers are available on request.

2.10. Histological analysis of tissues

Paraffin-embedded adipose tissues were cut into 5 μm thick sections, adhered onto glass slides, deparaffinized, and rehydrated by decreasing ethanol concentrations. Tissue-embedded slides were stained with hematoxylin and eosin (H&E). For immuno-histochemistry, rehydrated tissues were washed with PBS, boiled in a Citrate solution, and blocked with 4% serum before overnight incubation at 4 °C with primary antibodies against Ucp1 (ab23841-R, 1:500). Horseradish peroxidase labeled secondary antibodies were used (SP-9000, ZSGB-BIO). The slides were thoroughly washed and counterstained with hematoxylin, then examined under a microscope (Leica).

2.11. Luciferase reporter assay

For promoter luciferase reporter assay, full length miR-203 promoter (1480 bp) including two predicted binding sites was amplified from normal mouse genomic DNA (Toyobo) and cloned into PGL3-Basic vector (Promega). The two truncated vectors with different promoter lengths were also amplified from genomic DNA. The specific site mutated vector was constructed by HUADA genes. The pcDNA-C/EBPβ plasmid was preserved in our laboratory.3T3-L1 or 293T cells were seeded in 24-well plates (NEST) at an appropriate density one day before transfection. 300 ng each reporter construct were co-transfected with 2 ng renilla per well. Luciferase activity was measured at 36 h after transfection via a dual luciferase reporter assay kits (Promega), with firefly luciferase activity normalized to renilla activity.

For miR-203 binding luciferase reporter assay, 293T cells were seeded in 24-well plates (NEST) at an appropriate density one day before transfection. Two sequences including predicted binding sites on the Lyn 3′UTR were cloned into psiCheck-2 vector respectively (Promega). The specific site mutated sequences were processed by SANGON (Shanghai, China) and also cloned into psiCheck-2 vector. 100 ng reporter construct was co-transfected with 50 nM miR-203 mimic or a mimic control (GenePharma) into 293T cells using Lipofectamine 2000 according to the manufacturer's protocol (Invitrogen). Renilla and Firefly luciferase signals were measured at 48 h post-transfection via the Dual-Luciferase Reporter Assay kits (Promega).

2.12. Body temperature and body weight

8-week-old mice were housed at 4 °C for 48 h. The rectal body temperature was recorded at indicated time with a thermometer probe (BAT-12, PHYSITEMP INSTRUMENTS INC). Body weight and food intake mice were measured every week or before sacrifice.

2.13. Glucose and insulin tolerance tests

For the glucose tolerance test (GTT), mice were fasted overnight, followed by intraperitoneal glucose injection (2 mg/g body weight), and tail blood glucose levels were monitored at the indicated time. For the insulin tolerance test (ITT), mice fed ad libitum, followed by intraperitoneal human insulin injection (Novo Nordisk) (0.75 mU/g body weight) at around 2 p.m, and tail blood glucose levels were monitored at the indicated time.

2.14. Flow cytometry analysis

After isolation of adipose SVFs, single-cell were resuspended in PBS/3% BSA (FACS buffer) and treated with anti-CD16/32 for 15 min at 4 °C to block non-specific binding. Macrophages staining was performed for 15 min at 4 °C using the following antibodies: CD45, F4/80, CD11c, CD206 (Bioscience). Flow cytometry analysis was performed using a FACS instrument (BD Bioscience) to measure the fluorescence intensity.

2.15. Statistical analysis

Results are expressed as mean ± S.E.M Comparisons between groups were made by unpaired two-tailed Student's t-test, where $P < 0.05$ was considered as statistically significant.

3. RESULTS

3.1. MiR-203 expression positively correlates with energy expenditure

Our previous work demonstrated that microRNAs are required for feature maintenance and differentiation of brown adipocytes using tissue-specific Dgcr8 knockout mice [13]. With microarray analysis and experiment *in vitro*, we found that miR-203 may be a candidate for BAT activity. We confirmed that miR-203 expression was significantly induced in interscapular brown adipose tissue (iBAT) and sub-WAT after 4 °C cold exposure (Figure 1A) or with a β3-adrenoceptor agonist CL-316243(CL) treatment (Figure1B). Therefore, miR-203 expression is positively correlated with enhanced energy expenditure in adipose tissue. Additionally, we illustrated that the expression of miR-203 mainly existed in differentiated adipocytes compared to pre-adipocytes (Figure 1C). Similarly, miR-203 was highly expressed in mature adipocytes isolated from sub-WAT and iBAT rather than SVFs (Figure 1D).

To examine whether miR-203 was affected by obesity, we detected miR-203 expression in mice fed with HFD. Interestingly, miR-203 was

 © 2019 The Authors. Published by Elsevier GmbH. This is an open access article under the CC BY-NC-ND license (http://creativecommons.org/licenses/by-nc-nd/4.0/).

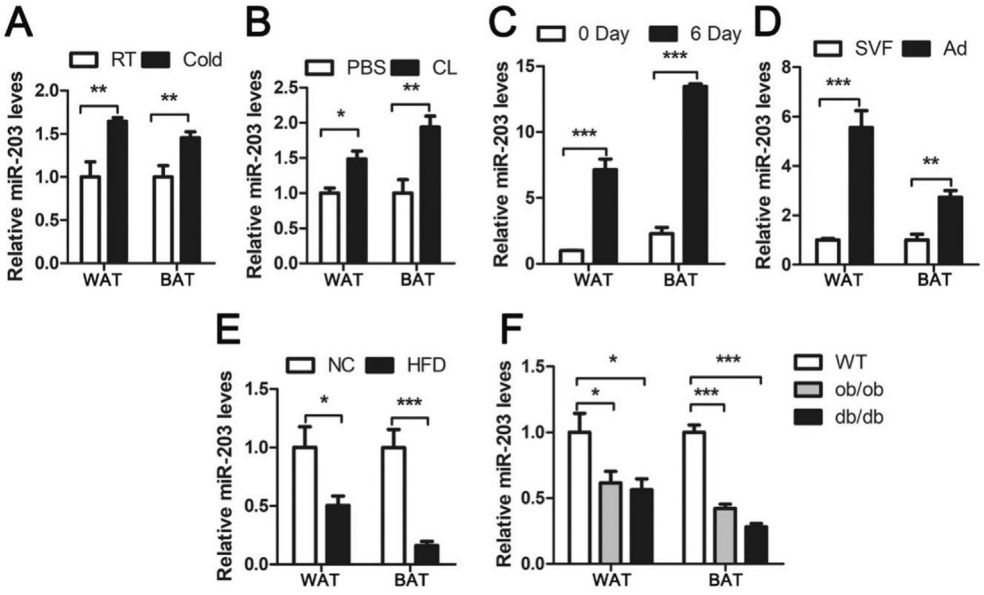

Figure 1: miR-203 expression positively correlates with energy expenditure. A, B qPCR analysis of *miR-203* in sub-WAT and iBAT from 1-week 4 °C-treated or 1-week CL-316243 treated mice compared to respective controls (n = 5/group). **C** qPCR analysis of *miR-203* in differentiated white and brown adipocytes compared to undifferentiated white and brown adipocytes isolated from sub-WAT or iBAT, respectively (n = 4/group). **D** qPCR analysis of *miR-203* in SVFs or mature adipocytes isolated from sub-WAT or iBAT, respectively, (n = 5/group). **E, F** qPCR analysis of *miR-203* in sub-WAT or iBAT from HFD (n = 5/group), ob/ob (n = 8/group) and db/db (n = 8/group) mice compared to respective controls, Sno-202 served as an internal control. *P < 0.05, **P < 0.01, and ***P < 0.001 by Student's t-test. Data presented as mean ± s.e.m.

markedly downregulated in sub-WAT and iBAT of mice upon HFD (Figure 1E). Consistent with these findings, miR-203 also decreased in the sub-WAT and iBAT of ob/ob and db/db mice (Figure 1F) comparing with wild type mice. These findings indicate that altered miR-203 expression may play a role in adipose tissue remodelingduring energy expenditure.

3.2. MiR-203 regulates subcutaneous white adipose tissue browning

To investigate the influence of miR-203 on thermogenic program, miR-203 inhibitor was injected into mouse inguinal fat and then these animals were housed in 4 °C or room temperature (RT) for 24 h before sacrifice (Figure 2A). MiR-203 was markedly reduced in sub-WAT injected with miR-203 inhibitor (Figure 2B). Although major brown fat markers such as Ucp1 and Pgc1α were markedly increased upon cold exposure, the extent of induction was significantly attenuated in miR-203 knockdown adipose tissue compared with the control samples (Figure 2C). Western blot also confirmed that the blunted induction of Ucp1 expression was present in miR-203 knockdown sub-WAT after cold exposure (Figure 2D). In contrast to the changes observed in brown fat markers, the expression of adipogenesis genes was less influenced by miR-203 knockdown (Figure 2C). To further confirm the effects of miR-203 inhibition on white fat browning, we knocked down miR-203 with miR-203-sponge adenoviral and exposed mice to 4 °C for 24 h (Figure 2E). Consistent with the inhibitor experiment, the mRNA levels of browning markers and protein level of Ucp1 were markedly reduced in miR-203-sponge injected sub-WAT (Figure 2F, G). H&E staining and immunostaining analysis indicated that the lipid droplet in adipocytes waslarger and the number of Ucp1 positive cells was lower in miR-203 knockdown sub-WAT (Figure 2H). Although knockdown of miR-203 did not change the body weight (Figure 2J) and inguinal fat mass in the short term (Supplemental Figure 1A, B), inhibiting miR-203 did impair body thermogenic response, as the body temperature of the miR-203 knockdown mice was lower than that of control animals upon cold exposure (Figure 2I).

In order to investigate the influence of miR-203 overexpression on thermogenic program and exclude the influence of sympathetic activation, mice were forced to express miR-203 with the adenovirus and recovered without cold exposure (Figure 2K). We found that the level of miR-203 was upregulated by adenovirus injection (Supplemental Fig. 1C). Notably, several browning markers and protein level of Ucp1 were elevated by miR-203 overexpression (Figure 2L, M). These data indicate that miR-203 has the potential to regulate thermogenic program in sub-WAT.

3.3. cAMP signaling promotes miR-203 expression through C/EBPβ

Our data demonstrate that miR-203 up-regulation is linked to cold stimulation. Upon cold stimulation, the sympathetic nervous system is activated to elevate intracellular cAMP levels, which promotes lipolysis as well as the up-regulation of Ucp1 in white adipose tissue. To examine the role of cAMP signaling in miR-203 expression, differentiated 3T3-L1 adipocyteswere treated with forskolin, a cAMP agonist. Forskolin significantly increased the expression of miR-203 and Ucp1 (Figure 3B) (Figure 3A, D). In order to identify which specific regulator is involved in cAMP signaling andmiR-203 expression, the pri-miR-203 promoter was explored through transcriptional factor prediction tool Generatrix, and two potential binding sites of C/EBPβ were found. Consistently, forskolin could promote C/EBPβ expression in mRNA and protein levels (Figure 3C, D). We also observed similar results in 3T3-L1 adipocytes treated with isoproterenol, a β3 adrenergic receptor agonist (Figure 3E, F, G & H).

Notably, the miR-203 expression was also robustly induced in differentiated white adipocytes by C/EBPβ overexpression (Figure 3I). The luciferase reporter with pri-miR-203 promoter was constructed (Figure 3J) and transfected into 3T3-L1 or 293T cell lines,

 © 2019 The Authors. Published by Elsevier GmbH. This is an open access article under the CC BY-NC-ND license (http://creativecommons.org/licenses/by-nc-nd/4.0/).

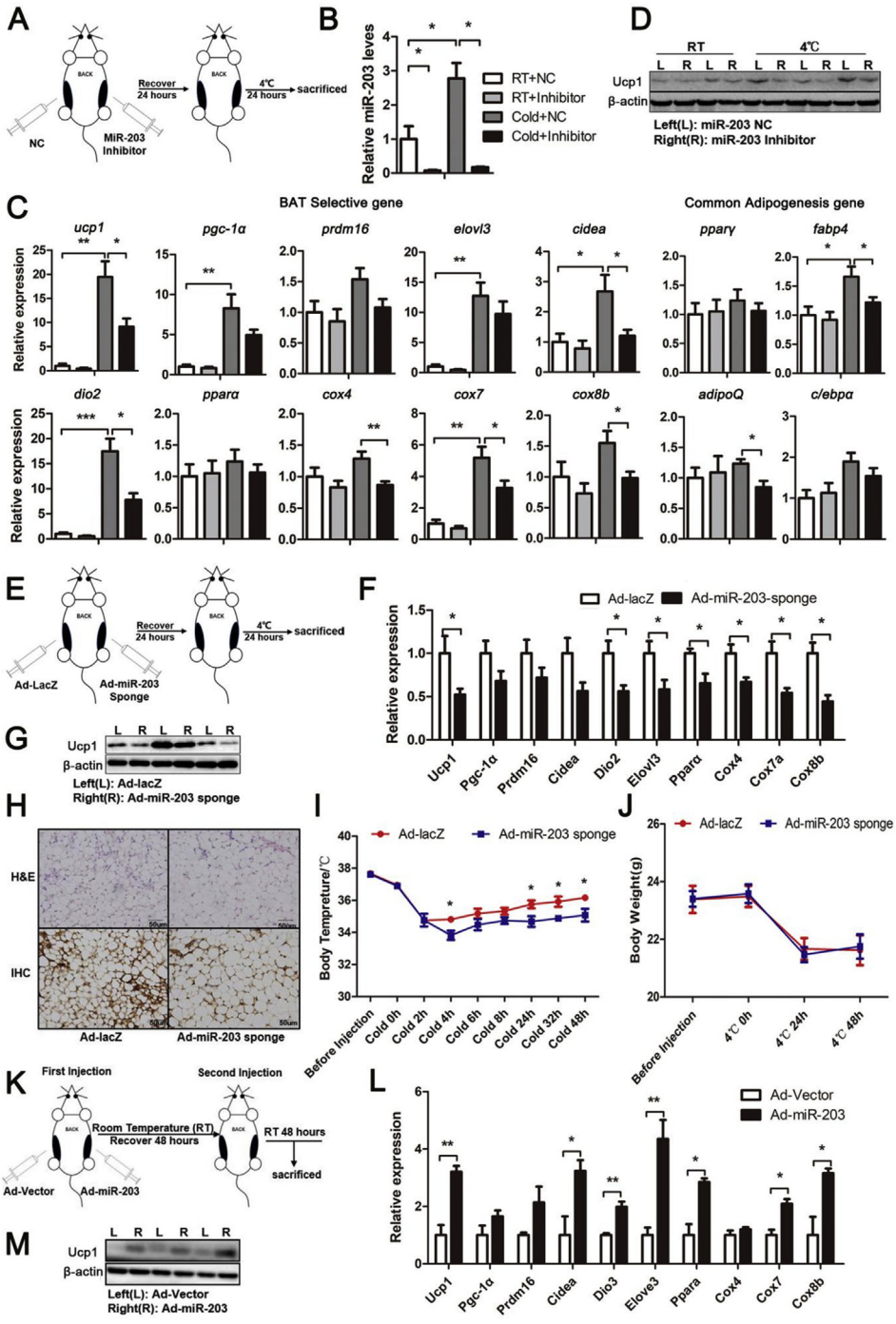

Figure 2: MiR-203 regulates subcutaneous white adipose tissue browning. A Schematic shows the inhibitor injection strategy used in figure (B), (C) and (D). Mice recovered for 24 h after injection and housed in room temperature (RT) (n = 5/group) or 4 °C, respectively (n = 7/group) for 24 h and then sacrificed. **B** qPCR analysis of *miR-203* in inhibitor injected sub-WAT from mice housed in RT (n = 5/group) or 4 °C (n = 7/group) (24hr) compared with control side. **C** qPCR analysis of BAT selective genes (*ucp1*, *pgc1α*, *prdm16*, *cidea*, *dio2*, *elovl3*, *pparα*, *cox4*, *cox7a*, *and cox8b*) and common adipogenesis genes (*pparγ*, *fabp4*, *adipoQ*, *c/ebpα*) in miR-203 inhibitor injected sub-WAT from mice housed in RT (n = 5/group) or 4 °C (n = 7/group) (24hr) compared with control side. **D** Western blot analysis of Ucp1 in miR-203 inhibitor injected sub-WAT from mice housed in RT or 4 °C (24hr) compared with control side. **E** Schematic shows the Ad-miR-203 sponge injection strategy used in figure (F), (G) and (H). Mice recovered for 24 h after injection and accepted 4 °C cold exposure for 24 h and then sacrificed (n = 8/group). **F** qPCR analysis of BAT selective genes (*ucp1*, *pgc1α*, *prdm16*, *cidea*, *dio2*, *elovl3*, *pparα*, *cox4*, *cox7a*, *and cox8b*) in miR-203 sponge injected sub-WAT from 4 °C treated mice (24hr) compared with Ad-lacZ injected side (n = 8/group). **G** Western blot analysis of Ucp1 in miR-203 sponge injected sub-WAT from 4 °C treated mice (24hr) compared with Ad-lacZ injected side. **H** Histological analysis of adipocyte morphology (H&E) and Ucp1 expression (IHC) in Ad-lacZ- and miR-203 sponge injected sub-WAT from 4 °C treated mice (24hr) (n = 3/group). **I, J** Body temperatures (°C) and body weights of Ad-lacZ or miR-203 sponge injected mice upon 4 °C treated (48hr) are shown (n = 6/group). **K** Schematic shows the Ad-miR-203 injection strategy used in figure (L) and (M). **L** qPCR analysis of BAT selective genes (*ucp1*, *pgc1α*, *prdm16*, *cidea*, *dio2*, *elovl3*, *pparα*, *cox4*, *cox7a*, *and cox8b*) in Ad-miR-203 injected sub-WAT from mice housed in RT (n = 6/group) compared with Ad-vector injected side. **M** Western blot analysis of Ucp1 in Ad-miR-203 injected sub-WAT from mice housed in RT compared with Ad-vector injected side. *P < 0.05, **P < 0.01, and ***P < 0.001 by Student's t-test. Data presented as mean ± s.e.m.

 © 2019 The Authors. Published by Elsevier GmbH. This is an open access article under the CC BY-NC-ND license (http://creativecommons.org/licenses/by-nc-nd/4.0/).

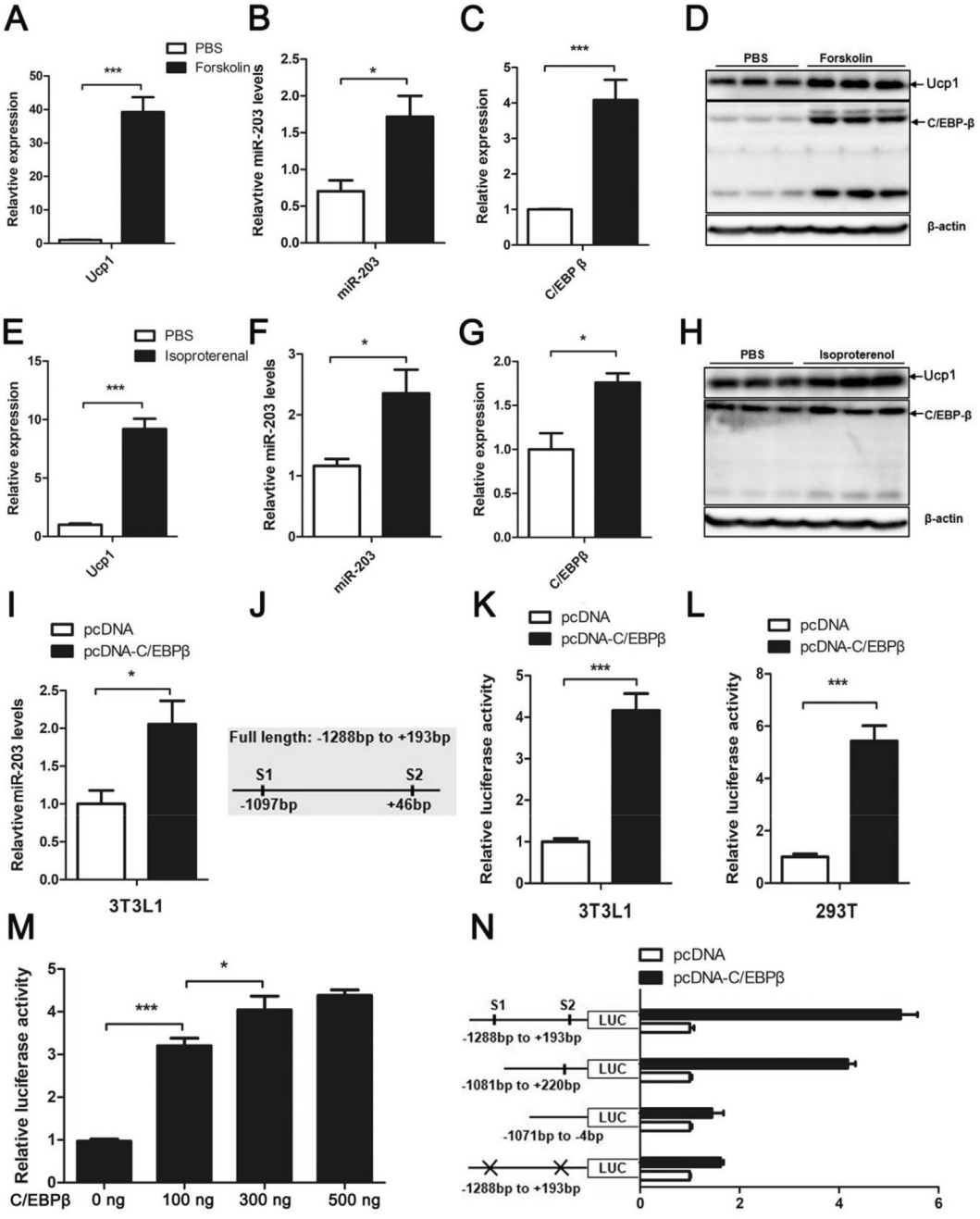

Figure 3: cAMP signaling promotes miR-203 expression through C/EBPβ. A, E qPCR analysis of *ucp1* in forskolin or isoproterenol treated 3T3-L1 adipocytes compared with PBS treated cells (n = 3/group). **B, F** qPCR analysis of *miR-203* in forskolin or isoproterenol treated 3T3-L1 adipocytes compared with PBS treated cells (n = 3/group). **C, G** qPCR analysis of *c/ebpβ* in forskolin or isoproterenol treated 3T3-L1 adipocytes compared with PBS treated cells (n = 3/group). **D, H** Western blot analysis of Ucp1 and C/EBPβ in forskolin or isoproterenol treated 3T3-L1 adipocytes compared with PBS treated cells. **I** qPCR analysis of *miR-203* in 3T3-L1 adipocytes with C/EBPβ overexpression compared with negative controls (n = 3/group). **J** Diagram to show the insert sequence and where C/EBPβ binding sites are in the promoter region of pri-miR-203; **K, L** Full length reporter construct was co-transfected with pcDNA-C/EBPβ vector in 3T3-L1 or 293T cells, After 36 h, luciferase activity was analyzed and plotted (n = 3/group). **M** Reporter constructs containing full length of miR-203 promoter were co-transfected with different concentration of pcDNA-C/EBPβ vector in 293T cells. After 36 h, luciferase activity was analyzed and plotted (n = 3/group). **N** Reporter constructs containing different length of miR-203 promoter or mutated construct were co-transfected with pcDNA-C/EBPβ vector in 293T cells. After 36 h, luciferase activity was analyzed and plotted (n = 3/group).*P < 0.05, **P < 0.01, and ***P < 0.001 by Student's t-test. Data presented as mean ± s.e.m.

andluciferase activity was increased in a dose dependent manner with C/EBPβ overexpression (Figure 3K, L & M). To further investigate the precise binding site of C/EBPβ in miR-203 promoter, we constructed two truncated and one mutational luciferase reporter constructs. With C/EBPβ overexpression, luciferase activity was markedly reduced in truncated and mutated groups compared with the full-length constructs (Figure 3N). Briefly, these data suggest that cAMP signaling promotes miR-203 expression through C/EBPβ.

 © 2019 The Authors. Published by Elsevier GmbH. This is an open access article under the CC BY-NC-ND license (http://creativecommons.org/licenses/by-nc-nd/4.0/).

3.4. MiR-203 represses IFN-γ signaling activation and reduces M1 macrophage infiltration

To gain detailed information about the targeted signal pathway by miR-203, we conducted RNA-seq on the miR-203 knockdown and control RNA samples of sub-WAT. Then, we performed a genome-wide mRNA profiling analysis. MiR-203 inhibition induced alterations in a range of biological processes; among the most upregulated ones were many IFN-γ signal pathway-related genes such as Stat1 and Stat2 (Figure 4A). Gene set enrichment analysis (GSEA) confirmed that GSEAs related to brown fat metabolism were repressed while the GSEAs related to interferon signal pathway were activated (Figure 4B, C). Q-PCR analysis successfully validated the down-regulation of

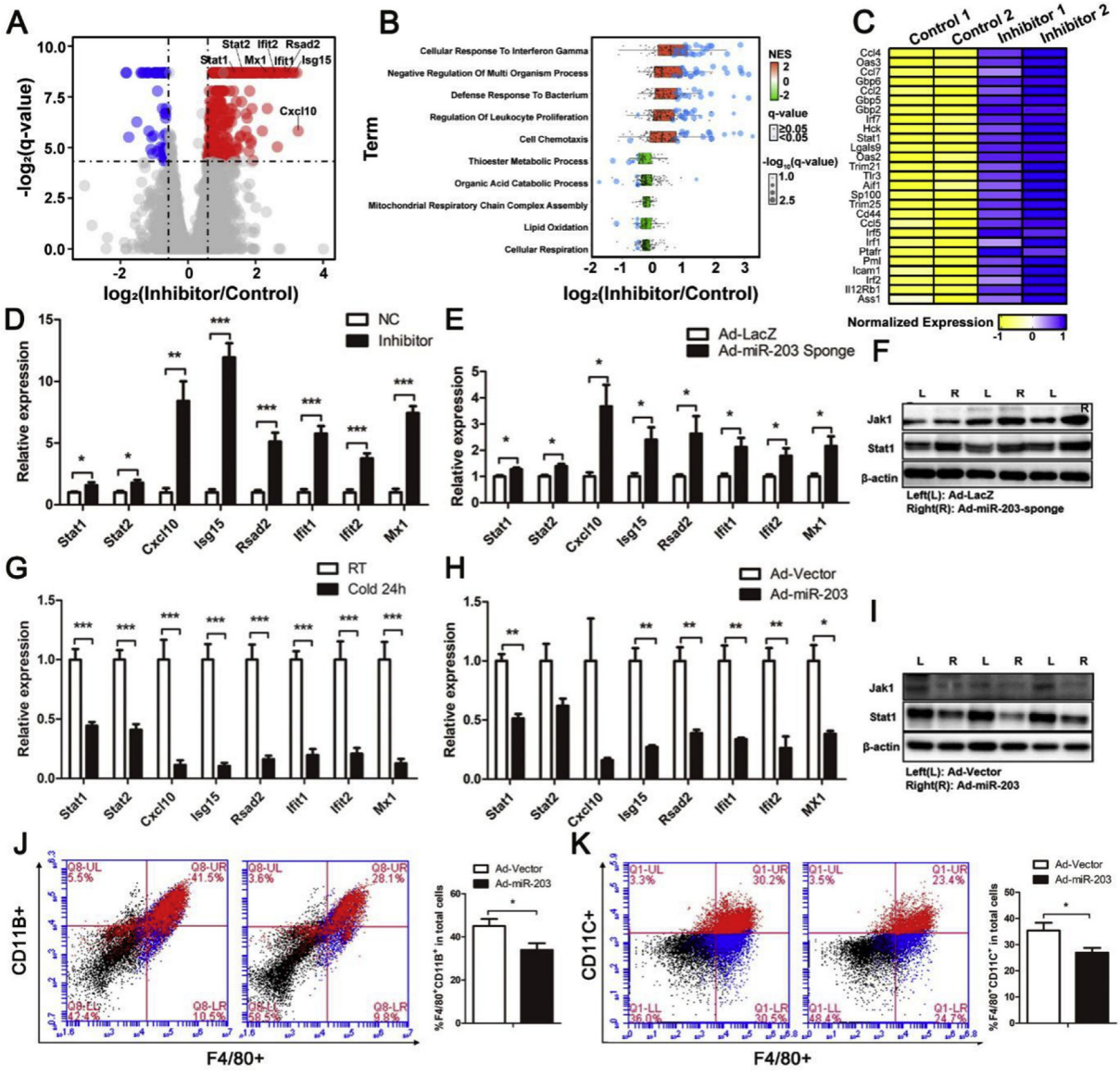

Figure 4: MiR-203 represses IFN-γ signaling activation and reduces M1 macrophage infiltration. A Volcano plot of all genes with detectable expression. Significantly up- and down-regulated genes have been colored in red and blue respectively. Genes involved in IFN-γ signaling processes, Stat1, Stat2, Mx1, Ifit2, Ifit1, Rsad2, Isg15, and Cxcl10, have been labeled on the volcano plot. **B** Top five most enriched up- and down-regulated biological processes obtained from GSEA analysis. Each boxplot represents the distribution of expression changes (log_2 (Mir-203_Inhibition/Control)) of all genes with detectable expression found within the respective gene set. Genes with significant q-value (q-value$<$0.05) are colored in blue and the level of significance is proportional to the size of the dot. The boxplot is colored by the level of normalized enrichment score (NES), with red and green representing up- and down-regulated processes. **C** Heatmap depicting expression changes of the genes included in the gene set of "Cellular Response to Interferon Gamma" biological pathway between control and Mir-203 inhibition. Only genes with q-value$<$0.05 have been included. Down- and up-regulated genes are colored by yellow and blue respectively. **D** qPCR analysis of IFN-γ signal pathway (*stat1*, *stat2*, *cxcl10*, *isg15*, *rsad2*, *ifit1*, *ifit2*, and *mx1*) in miR-203 inhibitor injected sub-WAT from 4 °C treated mice (24hr) compared with NC side (n = 7/group). **E** qPCR analysis of IFN-γ signal pathway (*stat1*, *stat2*, *cxcl10*, *isg15*, *rsad2*, *ifit1*, *ifit2*, and *mx1*) in miR-203-sponge injected sub-WAT from 4 °C treated mice (24hr) compared with Ad-lacZ injected side (n = 8/group). **F** Western blot analysis of Jak1 and Stat1 in miR-203-sponge injected sub-WAT from 4 °C treated mice (24hr) compared with Ad-lacZ injected side. **G** qPCR analysis of IFN-γ signal pathway (*stat1*, *stat2*, *cxcl10*, *isg15*, *rsad2*, *ifit1*, *ifit2*, and *mx1*) in sub-WAT from mice housed in 4 °C (n = 7/group)or room temperature (n = 5/group). **H** qPCR analysis of IFN-γ signal pathway (*stat1*, *stat2*, *cxcl10*, *isg15*, *rsad2*, *ifit1*, *ifit2*, and *mx1*) in Ad-miR-203 injected sub-WAT from mice housed in RT (n = 6/group) compared with Ad-vector injected side. **I** Western blot analysis of Jak1 and Stat1 in Ad-miR-203 injected sub-WAT from mice housed in RT compared with Ad-vector injected side. **J, K** The adipose total macrophages (F4/80 + CD11b+) and M1 macrophages (F4/80 + CD11c+) from SVFs were examined by flow cytometry analysis (n = 5/group).*P $<$ 0.05, **P $<$ 0.01, and ***P $<$ 0.001 by Student's t-test. Data presented as mean ± s.e.m.

 © 2019 The Authors. Published by Elsevier GmbH. This is an open access article under the CC BY-NC-ND license (http://creativecommons.org/licenses/by-nc-nd/4.0/).

brown fat markers and up-regulation of IFN-γ signal-related genes (Figures 2C & 4D). We observed accordant results in the miR-203-sponge injected sub-WAT in which IFN-γ induced genes such as Jak1 and Stat1 were increased at the mRNA and protein levels (Figure 4E, F). Conversely, the inflammation related IFN-γ signal pathway was strongly repressed by cold exposure (Figure 4G). This beneficial situation may be attributed to the activation of sympathetic and increased miR-203 level partly. Similar results were obtained by forced expression of miR-203 in inguinal fat at room temperature (Figure 4H, I), which almost excludes the influences of sympathetic activation. These results demonstrate that IFN-γ signaling severely disturbs white-to-brown conversion, and suppression of IFN-γ signaling significantly enhances the browning process [17]. These data suggest that miR-203 could be a linker connecting sympathetic nervous system and IFN-γ signaling activation.

Because IFN-γ signaling is a potent stimulus to drive M1 polarization and elicits the production of inflammatory mediators [28], we evaluated the proportion of macrophages in sub-WAT, Although the M2 (F4/80 + CD206+) macrophage content did not change (Supplemental Fig. 1D), quantification of FACS data revealed a significant reduce of total macrophage (F4/80 + CD11b+) and M1 macrophage (F4/80 + CD11c+) infiltration in the sub-WAT by miR-203 overexpression (Figure 4J, K). These data suggest that up-regulation of miR-203 repressesIFN-γ signaling activation and attenuates M1 macrophages infiltration.

3.5. MiR-203 directly blocks Lyn expression and inhibits Jak1-Stat1 signal pathway

Since miR-203 regulated Jak1-Stat1 signal pathway, we suspected miR-203 might directly target Jak1 or Stat1. However, the luciferase reporter assay with the putative miR-203 binding site of Jak1 or Stat1 did not support our hypothesis (Supplemental Figs. 1E and F). Then we screened for the upstream signaling of Jak1-Stat1 and found that knockdown of miR-203 significantly increased the expression of a Src family tyrosine kinase, Lyn (Figure 5A,B), which can directly trigger Jak1-Stat1 [21,29]. Conversely, the forced expression of miR-203 strongly repressed Lyn expression (Figure 5C, D). Based on microRNA target prediction tool (microRNA.org), Lyn may be a direct target of miR-203 (Figure 5E), and we found that miR-203 significantly repressed the luciferase activity with vectors containing a high score miR-203 binding site (bs1) of Lyn 3′UTR but did not affect the luciferase activity with vectors containing mutated binding sites or a low score miR-203 binding site (bs2) (Figure 5F).

To investigate the influence of Lyn on Jak1-Stat1 signaling activation, a Lyn inhibitor, Saracatinib, was injected into sub-WAT and the expression of Lyn was down-regulated (Figure 5G). Notably, the expression of Jak1 was strongly repressed in sub-WAT by Saracatinib (Figure 5H, I). Although the protein level of Stat1 was slightly reduced, our findings suggest a clearly effect of Lyn on Jak1-Stat1 signaling.

Previous studies show that miR-203 could be secreted into plasma [30]. In adipose tissue, miR-203 is mainly expressed in mature adipocytes (Figure 1D), but IFNγ is mainly secreted by T cells and NK cells [31]. In order to clarify the communication of miR-203 and IFNγsignaling among adipocytes and non-adipocytes, Jurkat cells were cultured with conditional medium (CM) from adipocytes overexpressing miR-203 or control adipocytes. We found that the expression of Lyn and protein level of Jak1 were strongly repressed in CM of adipocytes overexpressing miR-203 compared with controls (Figure 5J,K). We also found that the expression of Lyn and protein level of Jak1 were down-regulated when Jurkat cells were transfected with miR-203 mimics (Figure 5L, M) [21]. These results suggest that miR-203 could repress Jak1 expression through Lyn *in vivo* and *vitro*.

3.6. MiR-203 overexpression defends against obesity and improves glucose tolerance

Diet-induced obesity is associated with loss of tissue homeostasis and development of type 1 inflammatory responses in adipose tissue, characterized by IFN-γ induction. We found that the expression of Lyn and IFN-γ signaling were induced in HFD induced obese mice. (Figure 6A—C). These data suggest that the decreased miR-203 expression may contribute to activation of IFN-γ signal pathway.

To investigate whether miR-203 overexpression can be manipulated to improve metabolic homeostasis in HFD induced obesity, mice were injected with an adenovirus overexpressing miR-203 (Figure 6D); the injection was into inguinal fat of mice fed a ND or HFD for 12 weeks (twice/week). Forced expression of miR-203 did not affect body weight and glucose homeostasis under the ND condition (Figure 6E—I). However, up-regulation of miR-203 did protect mice against HFD induced obesity as these mice had lower body weight and less inguinal fat accumulation (Figure 6E,F). Overexpression of miR-203 improved glucose tolerance (Figure 6G) and insulin sensitivity (Figure 6H), and the insulin-signaling pathway was also enhanced in HFD fed mice (Figure 6I). Notably, protein levels of Lyn and Stat1 were strongly repressed by miR-203 overexpression (Figure 6J), and the negative influence of miR-203 on serum IFN-γ level also validated by ELISA in HFD fed mice (Figure 6K). In the current study, we propose a model in which miR-203 plays a role in controlling IFN-γ signaling (Figure 6L). These findings provide a novel insight into the role of miR-203 in regulating glucose tolerance and whole-body metabolic homeostasis through IFN-γ signaling suppression.

4. DISCUSSION

Brown and beige adipocytes attract great interest due to their favorable characters and therapeutic significance [32,33]. The recent confirmation that adult humans have brown adipose tissue has transformed our understanding of how adipose tissue regulates metabolism and energy balance [34,35]. Many researchers emphasize that fat burning in adipose tissue can improve obesity induced metabolic impairment [36,37]. In fact, inflammation and the immune system also play essential role in energy expenditure and metabolic syndrome [38—40]. The IFN-γ signaling pathway is one of the most important inflammatory pathways involved in obesity as it is associated chronic low-level inflammation and metabolic impairments [41,42]. The activation of the IFN-γ signaling pathway attenuates insulin sensitivity and results in metabolic disorder via sustained Jak1-Stat1 pathway activation [43]. Previous work has suggested that IFN-γ stimulated genes directly repressed the expression of Ucp1 andthermogenic-related genes [17]. Interestingly, the ectopic activation of type I IFN signaling in brown adipocytes induces mitochondrial dysfunction and reduces Ucp1 expression [18]. These data suggest that regulation of IFN signaling has an important influence on sub-WAT browning. We found that miR-203 was up-regulated in subcutaneous white fat browningand RNA-seq analysis showed that the IFN-γ signaling pathway was significantly activated under miR-203 inhibition. *In vivo*, overexpression of miR-203 also repressed the IFN-γ signaling pathway and enhanced the thermogenic program in ND fed mice. Mechanistically, miR-203 targeted tyrosine-protein kinase Lyn, an activator of Jak1-Stat1 [21,29,44] and repressed IFN-γ signal pathway which enhances sub-WAT browning ultimately. Unfortunately, in HFD fed mice we did not observe the same upregulation of thermogenic

 © 2019 The Authors. Published by Elsevier GmbH. This is an open access article under the CC BY-NC-ND license (http://creativecommons.org/licenses/by-nc-nd/4.0/).

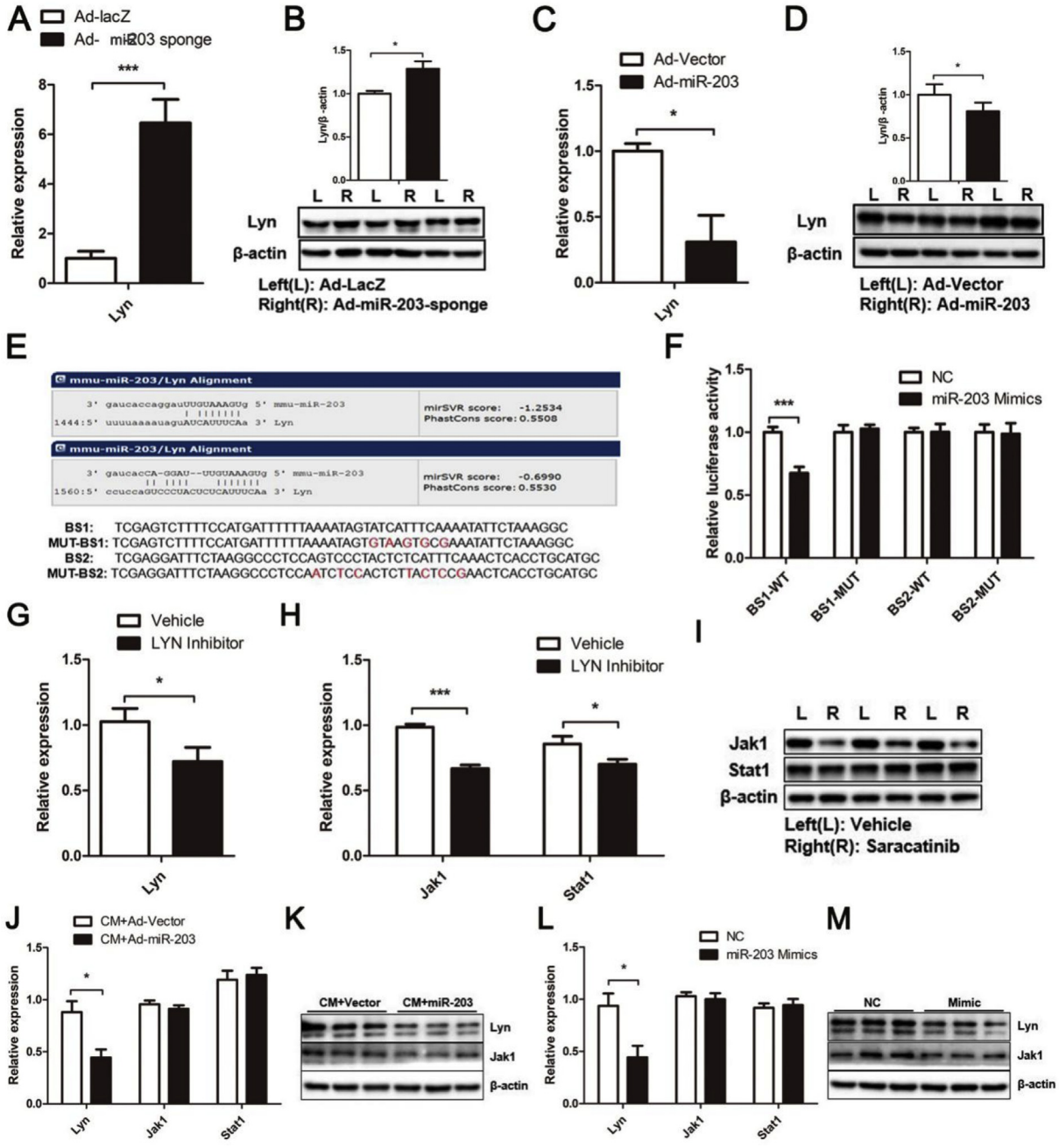

Figure 5: MiR-203 directly blocks Lyn expression and inhibits Jak1-Stat1 signal pathway. A qPCR analysis of *lyn* in miR-203-sponge injected sub-WAT from 4 °C treated mice (24hr) compared to Ad-lacZ injected side (n = 8/group). **B** Western blot analysis and quantification of Lyn in miR-203-sponge injected sub-WAT from 4 °C treated mice (24hr) compared to Ad-lacZ injected side. **C** qPCR analysis of *lyn* in Ad-miR-203 injected sub-WAT from mice housed in RT (n = 6/group) compared with Ad-vector injected side. **D** Western blot analysis and quantification of Lyn in Ad-miR-203 injected sub-WAT from mice housed in RT compared with Ad-vector injected side. **E** Upper panel: Alignment details of miR-203 to Lyn 3′ UTR binding site 1 (bs1) and binding site 2 (bs2). Lower panel: red mark nucleotides in bs1 and bs2 that were mutated to generate Mut-bs1 and Mut-bs2 constructs. **F** MiR-203 mimics or NC were co-transfected with psiCHECK2-Lyn-bs1, psiCHECK2-Lyn-Mut-bs1, psiCHECK2-Lyn-bs2 and psiCHECK2-Mut-bs2 vectors in 293T cell. After 48 h, renilla luciferase activity was quantified and normalized to firefly luciferase activity (n = 3/group). **G, H**qPCR analysis the mRNA levels of *lyn*, *jak1*, and *stat1* in sub-WAT derived from Saracatinib injected side compared with control side (n = 6/group). **I** Western blot analysis of Jak1 and Stat1 in sub-WAT derived from Saracatinib injected side compared with control side. **J** qPCR analysis the mRNA levels of *lyn*, *jak1*, and *stat1* in Jurkat cellscultured with conditional medium from miR-203 overexpression adipocytes compared with control adipocytes (n = 6/group). **K** Western blot analysis of Lyn and Jak1 in Jurkat cellscultured with conditional medium from miR-203 overexpression adipocytes compared with controladipocytes. **L** qPCR analysis the mRNA levels of *lyn*, *jak1* and *stat1* in Jurkat cellstransfected with miR-203 mimicscompared with control group (n = 6/group). **M** Western blot analysis of Lyn and Jak1 in Jurkat cellstransfected with miR-203 mimicscompared with control group. *P < 0.05, **P < 0.01, and ***P < 0.001 by Student's t-test. Data presented as mean ± s.e.m.

 © 2019 The Authors. Published by Elsevier GmbH. This is an open access article under the CC BY-NC-ND license (http://creativecommons.org/licenses/by-nc-nd/4.0/).

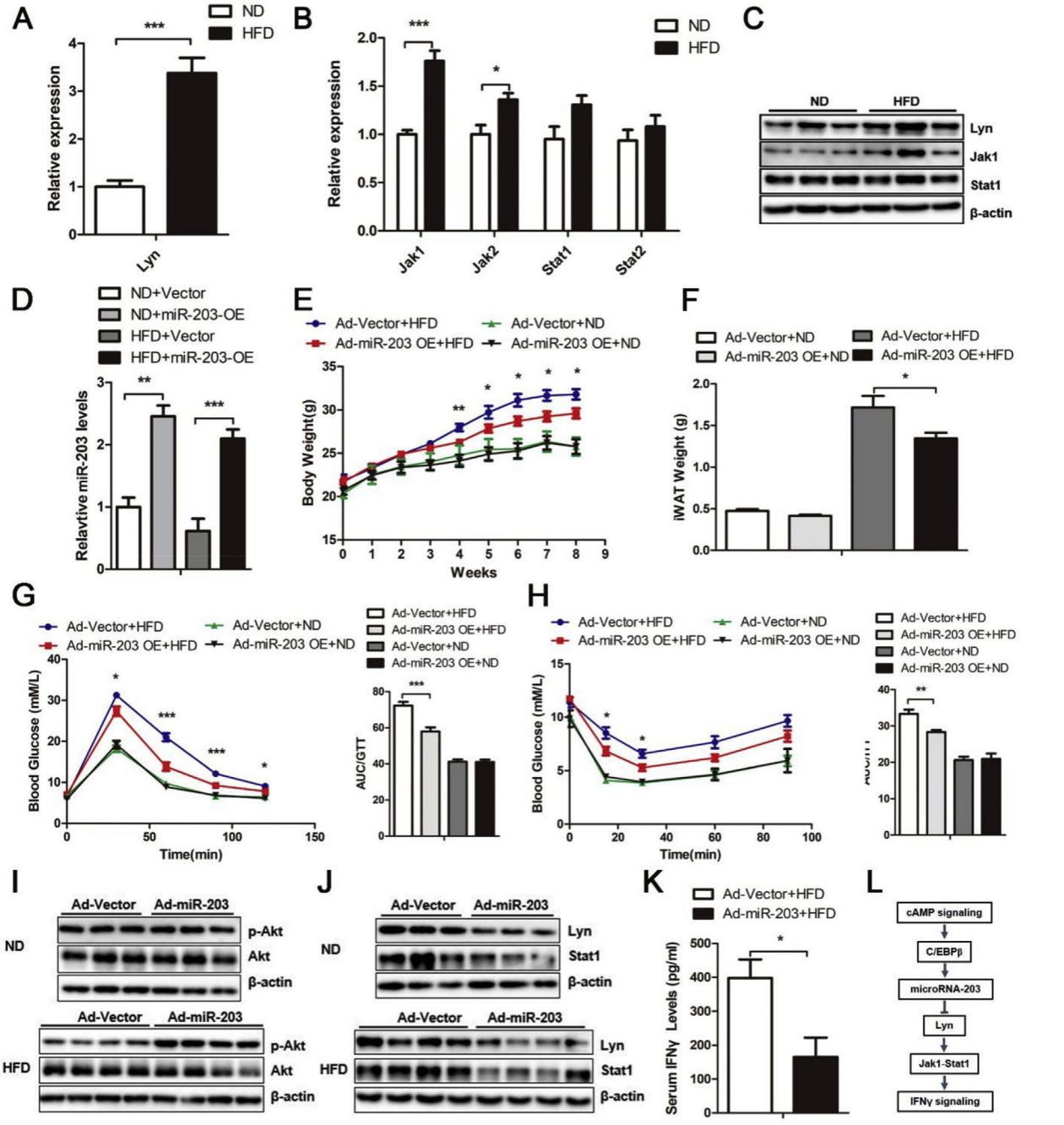

Figure 6: MiR-203 overexpression defends against obesity and improves glucose tolerance. A, B qPCR analysis the mRNA levels of *lyn* andIFN-γ signal pathway in sub-WAT derived from HFD mice compared with normal chow (n = 6/group). **C**Western blot analysis of Lyn, Jak1, and Stat1 in sub-WAT derived from HFD mice compared with normal chow. **D** qPCR analysis of *miR-203* expression in Ad-miR-203 injected sub-WAT from mice feeding HFD (n = 8/group) or ND (n = 6/group) compared with Ad-vector injected mice respectively. **E** Body weightsof Ad-miR-203 injected (twice a week) mice feeding HFD (n = 8/group) or ND (n = 6/group) compared with Ad-Vector injected mice respectively. For Ad-Vector + HFD group vs. Ad-miR-203 + HFD group: *P < 0.05; **P < 0.01. **F**sub-WAT weights of Ad-miR-203 injected mice feeding HFD (n = 8/group) or ND (n = 6/group) compared with Ad-Vector injected mice respectively. **G, H** GTT and ITT assays were conducted among Ad-miR-203 and Ad-Vector injected mice feeding HFD (n = 8/group) or ND (n = 6/group). For Ad-Vector + HFD group vs. Ad-miR-203 + HFD group: *P < 0.05; **P < 0.01; ***P < 0.001. **I** Western blot analysis of p-Akt and Akt in Ad-miR-203 injected sub-WAT (twice a week) from mice feeding HFD or ND compared with Ad-Vector injected mice respectively. **J** Western blot analysis of Lyn and Stat1 in Ad-miR-203 injected sub-WAT from mice feeding HFD or ND compared with Ad-vector injected mice respectively. **K** Serum levels of IFN-γ among Ad-miR-203 and Ad-Vector injected mice feeding HFD were examined by ELISA kit (n = 8/group). **L** A working model for the cAMP-miR-203-IFN-γ network.*P < 0.05, **P < 0.01, and ***P < 0.001 by Student's t-test. Data presented as mean ± s.e.m.

 © 2019 The Authors. Published by Elsevier GmbH. This is an open access article under the CC BY-NC-ND license (http://creativecommons.org/licenses/by-nc-nd/4.0/).

genes as ND mice (Supplemental Fig. 1G) but still found a decrease of serum IFN-γ and animprovement in the insulin resistance. This may be attributed to the complex lipid metabolism environment between cold exposure and HFD feeding condition.

Recent studies in inflammation and immune system have revealed that targeting neuro-innate signaling may offer new approaches to mitigate chronic inflammation-induced metabolic impairments [14]. Physical exercise elicits a potent anti-inflammatory effect, which improves insulin sensitivity and lipid metabolism [45–50]. Cold exposure has many similarities to physical exercise and gives rise to sustained stimulation of the sympathetic nervous system, causing catecholamines release from synapse terminals and activation of cAMP signaling [51–53]. Our results show that cAMP signaling promotes miR-203 up-regulation which isconsistent with the expression being dependent upon C/EBPβ.The inflammation related IFN-γ signaling pathway was strongly repressed by cold exposure and the cAMP-miR-203-IFN-γ network did involve neuro-immuno-metabolic signaling. Our results show that miR-203is mainly expressed in adipocytes and responds to cAMP signaling. Meanwhile IFNγ is mainly secreted by T cells and NK cells in adipose tissue [31]. We tried to clarify the communication between miR-203 and IFN-γ among adipocytes and non-adipocytes and found that the expressions of Lyn and Jak1 in T cell were repressed through conditional medium experiments. However, we have not defined experimentally whether miR-203 is secreted from adipocytes through exosomes or in other ways; this needs further exploration. In brief, we declare that miR-203 acts as a messenger between thecAMP signaling pathway and the IFN-γ signaling pathway. This work supports the idea that targeting neuro-immuno-metabolic signaling between the sympathetic nervous system and the immune system may offer a new approach to ameliorate chronic inflammation-induced metabolic impairments.

In summary, our studyfinds that up-regulation of miR-203 could be used for the suppression of the IFN-γ signaling pathway. Our findings also provide mechanistic insights that the cAMP-miR-203-IFN-γ network regulates inflammation response and sub-WAT browning, which could be exploited for new therapies against obesity and metabolic syndrome.

AUTHOR CONTRIBUTIONS

Guo Xiaolong, Zhang Zhichun conducted experiments, analyzed data, and wrote manuscript. Zeng Ting, Lim Yen Ching, Wang Yumeng, Xie Xinxin, Yang Song, Huang Chenglong, Xu Min, Tao Linfen, Zeng Hongxiang conducted experiments and analyzed data. Li Xi, Sun Lei analyzed data and revised manuscript. Li Xi, Sun Lei are the guarantors of this work, and, as such, had full access to all the data in the study and takes responsibility for the integrity of the data and the accuracy of the data analysis.

ACKNOWLEDGEMENT

This work was supported by National Natural Science Foundation of China, China (81770861 and 31571401 to X. Li), Chong Qing Science and Technology Foundation, China (cstc2018jcyjAX0232 to X. Li), Chong Qing Education Foundation, China (KJZD-K201800402 to X. Li), Open Fund-Individual Research (OF-IRG), Singapore (NMRC/OFIRG/0062/2017 to L. Sun), Ministry of Education (MOE) Tier2 grant, Singapore (MOE2017-T2-2-015 to L. Sun) and Tanoto Initiative in Diabetes Research, Singapore (to L. Sun).

CONFLICT OF INTEREST

None declared.

APPENDIX A. SUPPLEMENTARY DATA

Supplementary data to this article can be found online at https://doi.org/10.1016/j.molmet.2019.07.002.

REFERENCES

[1] Collaborators GBDO, Afshin, A., Forouzanfar, M.H., Reitsma, M.B., Sur, P., Estep, K., et al., 2017. Health effects of overweight and obesity in 195 countries over 25 years. New England Journal of Medicine 377:13–27.

[2] Collaboration NCDRF, 2017. Worldwide trends in body-mass index, underweight, overweight, and obesity from 1975 to 2016: a pooled analysis of 2416 population-based measurement studies in 128.9 million children, adolescents, and adults. Lancet 390:2627–2642.

[3] Ikeda, K., Maretich, P., Kajimura, S., 2018. The common and distinct features of Brown and beige adipocytes. Trends in Endocrinology and Metabolism TEM 29:191–200.

[4] Kajimura, S., Spiegelman, B.M., Seale, P., 2015. Brown and beige fat: physiological roles beyond heat generation. Cell Metabolism 22:546–559.

[5] Harms, M., Seale, P., 2013. Brown and beige fat: development, function and therapeutic potential. Nature Medicine 19:1252–1263.

[6] Shinoda, K., Ohyama, K., Hasegawa, Y., Chang, H.Y., Ogura, M., Sato, A., et al., 2015. Phosphoproteomics identifies CK2 as a negative regulator of beige adipocyte thermogenesis and energy expenditure. Cell Metabolism 22:997–1008.

[7] Peirce, V., Carobbio, S., Vidal-Puig, A., 2014. The different shades of fat. Nature 510:76–83.

[8] Inagaki, T., Sakai, J., Kajimura, S., 2016. Transcriptional and epigenetic control of brown and beige adipose cell fate and function. Nature Reviews Molecular Cell Biology 17:480–495.

[9] Chen, Y., Pan, R., Pfeifer, A., 2017. Regulation of brown and beige fat by microRNAs. Pharmacology and Therapeutics 170:1–7.

[10] Arner, P., Kulyte, A., 2015. MicroRNA regulatory networks in human adipose tissue and obesity. Nature Reviews Endocrinology 11:276–288.

[11] Trajkovski, M., Ahmed, K., Esau, C.C., Stoffel, M., 2012. MyomiR-133 regulates brown fat differentiation through Prdm16. Nature Cell Biology 14:1330–1335.

[12] Chen, Y., Siegel, F., Kipschull, S., Haas, B., Frohlich, H., Meister, G., et al., 2013. miR-155 regulates differentiation of brown and beige adipocytes via a bistable circuit. Nature Communications 4:1769.

[13] Kim, H.J., Cho, H., Alexander, R., Patterson, H.C., Gu, M., Lo, K.A., et al., 2014. MicroRNAs are required for the feature maintenance and differentiation of brown adipocytes. Diabetes 63:4045–4056.

[14] Camell, C.D., Sander, J., Spadaro, O., Lee, A., Nguyen, K.Y., Wing, A., et al., 2017. Inflammasome-driven catecholamine catabolism in macrophages blunts lipolysis during ageing. Nature 550:119–123.

[15] Bachman, E.S., Dhillon, H., Zhang, C.Y., Cinti, S., Bianco, A.C., Kobilka, B.K., et al., 2002. betaAR signaling required for diet-induced thermogenesis and obesity resistance. Science 297:843–845.

[16] Cao, W., Daniel, K.W., Robidoux, J., Puigserver, P., Medvedev, A.V., Bai, X., et al., 2004. p38 mitogen-activated protein kinase is the central regulator of cyclic AMP-dependent transcription of the Brown fat uncoupling protein 1 gene. Molecular and Cellular Biology 24:3057–3067.

[17] Moisan, A., Lee, Y.K., Zhang, J.D., Hudak, C.S., Meyer, C.A., Prummer, M., et al., 2015. White-to-brown metabolic conversion of human adipocytes by JAK inhibition. Nature Cell Biology 17:57–67.

[18] Kissig, M., Ishibashi, J., Harms, M.J., Lim, H.W., Stine, R.R., Won, K.J., et al., 2017. PRDM16 represses the type I interferon response in adipocytes to promote mitochondrial and thermogenic programing. The EMBO Journal 36:1528–1542.

 © 2019 The Authors. Published by Elsevier GmbH. This is an open access article under the CC BY-NC-ND license (http://creativecommons.org/licenses/by-nc-nd/4.0/).

[19] Reardon, C.A., Lingaraju, A., Schoenfelt, K.Q., Zhou, G., Cui, C., Jacobs-El, H., et al., 2018. Obesity and insulin resistance promote atherosclerosis through an IFNγ-regulated macrophage protein network. Cell Reports 23:3021–3030.

[20] Sestan, M., Marinovic, S., Kavazovic, I., Cekinovic, D., Wueest, S., Turk Wensveen, T., et al., 2018. Virus-induced interferon-gamma causes insulin resistance in skeletal muscle and derails glycemic control in obesity. Immunity 49:164–177 e166.

[21] Dong, G., You, M., Ding, L., Fan, H., Liu, F., Ren, D., et al., 2015. STING negatively regulates double-stranded DNA-activated JAK1-STAT1 signaling via SHP-1/2 in B cells. Molecules and Cells 38:441–451.

[22] Sun, L., Xie, H., Mori, M.A., Alexander, R., Yuan, B., Hattangadi, S.M., et al., 2011. Mir193b-365 is essential for brown fat differentiation. Nature Cell Biology 13:958–965.

[23] Trapnell, C., Williams, B.A., Pertea, G., Mortazavi, A., Kwan, G., van Baren, M.J., et al., 2010. Transcript assembly and quantification by RNA-Seq reveals unannotated transcripts and isoform switching during cell differentiation. Nature Biotechnology 28:511–515.

[24] Trapnell, C., Roberts, A., Goff, L., Pertea, G., Kim, D., Kelley, D.R., et al., 2012. Differential gene and transcript expression analysis of RNA-seq experiments with TopHat and Cufflinks. Nature Protocols 7:562–578.

[25] Subramanian, A., Tamayo, P., Mootha, V.K., Mukherjee, S., Ebert, B.L., Gillette, M.A., et al., 2005. Gene set enrichment analysis: a knowledge-based approach for interpreting genome-wide expression profiles. Proceedings of the National Academy of Sciences of the United States of America 102:15545–15550.

[26] Liberzon, A., Subramanian, A., Pinchback, R., Thorvaldsdottir, H., Tamayo, P., Mesirov, J.P., 2011. Molecular signatures database (MSigDB) 3.0. Bioinformatics 27:1739–1740.

[27] Supek, F., Bosnjak, M., Skunca, N., Smuc, T., 2011. REVIGO summarizes and visualizes long lists of gene ontology terms. PLoS One 6:e21800.

[28] Rocha, V.Z., Folco, E.J., Sukhova, G., Shimizu, K., Gotsman, I., Vernon, A.H., et al., 2008. Interferon-gamma, a Th1 cytokine, regulates fat inflammation: a role for adaptive immunity in obesity. Circulation Research 103:467–476.

[29] Wang, L., Kurosaki, T., Corey, S.J., 2007. Engagement of the B-cell antigen receptor activates STAT through Lyn in a Jak-independent pathway. Oncogene 26:2851–2859.

[30] Okugawa, Y., Toiyama, Y., Hur, K., Yamamoto, A., Yin, C., Ide, S., et al., 2019. Circulating miR-203 derived from metastatic tissues promotes myopenia in colorectal cancer patients. Journal of Cachexia, Sarcopenia and Muscle.

[31] Ghazarian, M., Luck, H., Revelo, X.S., Winer, S., Winer, D.A., 2015. Immunopathology of adipose tissue during metabolic syndrome. Turkish Journal of Pathology.

[32] Wang, W., Seale, P., 2016. Control of brown and beige fat development. Nature Reviews Molecular Cell Biology 17:691–702.

[33] Kiefer, F.W., 2017. The significance of beige and brown fat in humans. Endocrine Connections 6:R70–R79.

[34] van Marken Lichtenbelt, W.D., Vanhommerig, J.W., Smulders, N.M., Drossaerts, J.M., Kemerink, G.J., Bouvy, N.D., et al., 2009. Cold-activated brown adipose tissue in healthy men. New England Journal of Medicine 360:1500–1508.

[35] Cypess, A.M., Lehman, S., Williams, G., Tal, I., Rodman, D., Goldfine, A.B., et al., 2009. Identification and importance of brown adipose tissue in adult humans. New England Journal of Medicine 360:1509–1517.

[36] Bartelt, A., Heeren, J., 2014. Adipose tissue browning and metabolic health. Nature Reviews Endocrinology 10:24–36.

[37] White, J.D., Dewal, R.S., Stanford, K.I., 2019. The beneficial effects of brown adipose tissue transplantation. Molecular Aspects of Medicine.

[38] Huang, Z., Zhong, L., Lee, J.T.H., Zhang, J., Wu, D., Geng, L., et al., 2017. The FGF21-CCL11 Axis mediates beiging of white adipose tissues by coupling sympathetic nervous system to type 2 immunity. Cell Metabolism 26:493–508 e494.

[39] Ruiz de Azua, I., Mancini, G., Srivastava, R.K., Rey, A.A., Cardinal, P., Tedesco, L., et al., 2017. Adipocyte cannabinoid receptor CB1 regulates energy homeostasis and alternatively activated macrophages. Journal of Clinical Investigation 127:4148–4162.

[40] Wolf, Y., Boura-Halfon, S., Cortese, N., Haimon, Z., Sar Shalom, H., Kuperman, Y., et al., 2017. Brown-adipose-tissue macrophages control tissue innervation and homeostatic energy expenditure. Nature Immunology 18:665–674.

[41] Vandanmagsar, B., Youm, Y.H., Ravussin, A., Galgani, J.E., Stadler, K., Mynatt, R.L., et al., 2011. The NLRP3 inflammasome instigates obesity-induced inflammation and insulin resistance. Nature Medicine 17:179–188.

[42] Wensveen, F.M., Valentic, S., Sestan, M., Turk Wensveen, T., Polic, B., 2015. The "Big Bang" in obese fat: events initiating obesity-induced adipose tissue inflammation. European Journal of Immunology 45:2446–2456.

[43] McGillicuddy, F.C., Chiquoine, E.H., Hinkle, C.C., Kim, R.J., Shah, R., Roche, H.M., et al., 2009. Interferon gamma attenuates insulin signaling, lipid storage, and differentiation in human adipocytes via activation of the JAK/STAT pathway. Journal of Biological Chemistry 284:31936–31944.

[44] Chang, Y.J., Holtzman, M.J., Chen, C.C., 2002. Interferon-gamma-induced epithelial ICAM-1 expression and monocyte adhesion. Involvement of protein kinase C-dependent c-Src tyrosine kinase activation pathway. Journal of Biological Chemistry 277:7118–7126.

[45] Lancaster, G.I., Febbraio, M.A., 2014. The immunomodulating role of exercise in metabolic disease. Trends in Immunology 35:262–269.

[46] Benatti, F.B., Pedersen, B.K., 2015. Exercise as an anti-inflammatory therapy for rheumatic diseases-myokine regulation. Nature Reviews Rheumatology 11:86–97.

[47] Perandini, L.A., de Sa-Pinto, A.L., Roschel, H., Benatti, F.B., Lima, F.R., Bonfa, E., et al., 2012. Exercise as a therapeutic tool to counteract inflammation and clinical symptoms in autoimmune rheumatic diseases. Autoimmunity Reviews 12:218–224.

[48] Mathur, N., Pedersen, B.K., 2008. Exercise as a mean to control low-grade systemic inflammation. Mediators of Inflammation 2008:1–6.

[49] Pedersen, B.K., 2006. The anti-inflammatory effect of exercise: its role in diabetes and cardiovascular disease control. Essays in Biochemistry 42:105–117.

[50] Improta Caria, A.C., Nonaka, C.K.V., Pereira, C.S., Soares, M.B.P., Macambira, S.G., Souza, B.S.F., 2018. Exercise training-induced changes in MicroRNAs: beneficial regulatory effects in hypertension, type 2 diabetes, and obesity. International Journal of Molecular Sciences 19.

[51] Zouhal, H., Jacob, C., Delamarche, P., Gratas-Delamarche, A., 2008. Catecholamines and the effects of exercise, training and gender. Sports Medicine 38:401–423.

[52] Christensen, N.J., Galbo, H., 1983. Sympathetic nervous activity during exercise. Annual Review of Physiology 45:139–153.

[53] Zouhal, H., Lemoine-Morel, S., Mathieu, M.E., Casazza, G.A., Jabbour, G., 2013. Catecholamines and obesity: effects of exercise and training. Sports Medicine 43:591–600.

 © 2019 The Authors. Published by Elsevier GmbH. This is an open access article under the CC BY-NC-ND license (http://creativecommons.org/licenses/by-nc-nd/4.0/).